

Three Clusters of Conformational States in P450cam Reveal a Multistep Pathway for Closing of the Substrate Access Channel^{†,‡}

Young-Tae Lee,[§] Edith C. Glazer,^{§,||} Richard F. Wilson,[§] C. David Stout, and David B. Goodin*

Department of Molecular Biology, 10550 North Torrey Pines Road, The Scripps Research Institute, La Jolla, California 92037, United States. [§]These authors contributed equally to this work. ^{||}Present address: Department of Chemistry, University of Kentucky, Lexington, KY 40506-0055.

Received October 27, 2010; Revised Manuscript Received December 17, 2010

ABSTRACT: Conformational changes in the substrate access channel have been observed for several forms of cytochrome P450, but the extent of conformational plasticity exhibited by a given isozyme has not been completely characterized. Here we present crystal structures of P450cam bound to a library of 12 active site probes containing a substrate analogue tethered to a variable linker. The structures provide a unique view of the range of protein conformations accessible during substrate binding. Principal component analysis of a total of 30 structures reveals three discrete clusters of conformations: closed (P450cam-C), intermediate (P450cam-I), and fully open (P450cam-O). Relative to P450cam-C, the P450cam-I state results predominantly from a retraction of helix F, while both helices F and G move in concert to reach the fully open P450cam-O state. Both P450cam-C and P450cam-I are well-defined states, while P450cam-O shows evidence of a somewhat broader distribution of conformations and includes the open form recently seen in the absence of substrate. The observed clustering of protein conformations over a wide range of ligand variants suggests a multistep closure of the enzyme around the substrate that begins by conformational selection from an ensemble of open conformations and proceeds through a well-defined intermediate, P450cam-I, before full closure to the P450cam-C state in the presence of small substrates. This multistep pathway may have significant implications for a full understanding of substrate specificity, kinetics, and coupling of substrate binding to P450 function.

Substrate recognition by cytochrome P450s has been intensively studied for many decades, and while much is known about how structural variations of these enzymes result in their wide ranging specificity, less is understood about the role played by protein dynamics and active site motion in this process. P450s are an important family of monooxygenases with more than 10000 members widely distributed in living systems from bacteria to humans (1). They use O₂ and a cysteine-coordinated heme to catalyze the oxidation of a vast array of substrates in reactions as diverse as steroid biosynthesis and xenobiotic metabolism (2). Even distantly related P450s share an overall conserved protein fold, first described for P450cam, CYP101A1, a camphor metabolizing P450 from *Pseudomonas putida* (3, 4). Despite this overall similarity, significant differences in the sequence, structure, of the substrate access channel and membrane location of individual P450s have been characterized. In addition, exactly how these differences allow some P450s to catalyze the stereospecific hydroxylation of a single well-defined substrate while others are able to oxidize a wide range of compounds remains incompletely understood (5, 6).

The diversity of substrate specificities of P450s is believed to result largely from differences in the structure, flexibility, and/or dynamics of the substrate binding channel that connects the

protein surface to the deeply buried heme center. The substrate binding channel is defined by antiparallel helices F and G, the intervening F–G loop, and segments of helix B', which fold over and around the heme and helix I to enclose the substrate and position it for attack by the reactive Compound I center of the heme (4, 7). There are significant differences in the sequence of these structural elements between various forms of P450 (8), and as a consequence, the structure of the substrate binding channel varies considerably from one form to another (9). Thus, the small, closed substrate access channels seen in many prokaryotic P450s (4, 10–12) are in marked contrast to the larger, more open channels seen for mammalian microsomal enzymes involved in drug metabolism (5, 13, 14).

Conformational change clearly plays an important role in substrate recognition for many if not all P450s, but only recently have specific details become available about the conformational space sampled by a given enzyme (15–18). For a number of P450s, most notably P450cam, the closed conformation observed for the camphor-bound state must undergo significant conformational change to allow binding of substrate and release of product (3, 4, 11). Importantly, reports have shown several examples of bacterial P450s that exist both in an open conformation in the absence of substrate and in a closed conformation in the presence of substrate or ligand (13, 16, 19–24). This now includes P450cam, which was previously observed in the closed conformation even in the absence of substrate (25), as we have recently reported an open conformation of P450cam when it is crystallized in the absence of substrate that is essentially identical to that observed in the presence of large tethered substrates (18).

[†]This work was supported by Grant GM41049 from the National Institutes of Health.

[‡]The atomic coordinates and structures factors were deposited in the Protein Data Bank as entries 3P6M, 3P6N, 3P6O, 3P6P, 3P6Q, 3P6R, 3P6S, 3P6T, 3P6U, 3P6V, 3P6W, and 3P6X.

*To whom correspondence should be addressed. Telephone: (858) 784-9892. Fax: (858) 784-2857. E-mail: dbg@scripps.edu.

This suggests that the open conformation does not result from being held open by the tethered substrate but is instead dynamically sampled in the substrate-free form. While channel closure is likely to influence regio- and/or stereospecificity of oxidation in these enzymes, it is unclear at present whether or how the functional activity of the enzyme is coupled to conformational state.

The role of active site flexibility in P450 substrate recognition is of considerable importance for mammalian P450s. Among the diverse and promiscuous drug-metabolizing microsomal enzymes, evidence both supporting and refuting conformational change associated with substrate binding exists. For example, CYP2B4 has been observed to undergo significant conformational change upon binding substrates or inhibitors (13, 14, 17), while CYP3A4 has been observed in both the substrate-bound and -free forms with relatively small changes in structure (26). For the highly specific mitochondrial CYP24A1, which is responsible for the specific hydroxylation of 1 α ,25-dihydroxyvitamin D₃, an open conformation was observed without bound substrate, and the importance of channel closure upon substrate binding remains unknown (27). Thus, a general concept that highly specific biosynthetic P450s may require a more closed and tight fit around the substrate has emerged, while the more promiscuous drug-metabolizing enzymes make use of a larger, more open, nonspecific active site channel.

Substrate recognition by P450s could be realized in a number of ways, ranging from a rigid lock-and-key interaction that matches a particular substrate to a complementary but static binding site to induced-fit models, in which substrate binding induces a protein conformational change that exists only upon interaction with substrate. Alternatively, conformational selection implies that substrate binds a subset of conformations from a preexisting ensemble of states, causing a shift in the equilibrium of populated states as the energy landscape changes upon substrate binding (28). Recent results for P450cam (18), EryK (15), PikC (16), and CYP119 (29), showing population of both open and closed conformations in the absence of substrates, strongly suggest that these enzymes make use of conformational selection by dynamically visiting alternate conformations. While these results show how substrates can gain access to the buried active sites, the full range of conformational states sampled by a given P450 or the details about the specific trajectories or conformational intermediates remain undefined. As these features are likely to be critically important for substrate recognition and specificity in this broad class of enzymes, it would be important to characterize the range of conformational states available to a given structure.

In this study, we report the structural characterization of P450cam bound to a family of related tethered substrates and describe the extent to which the protein responds to variations in the probe. The results described here provide direct observation of at least three distinct clusters of conformational substates termed P450cam-C¹ (closed), P450cam-I (intermediate), and P450cam-O (open) and suggest a stepwise pathway for the interconversion from the closed to the open state through a well-defined intermediate.

EXPERIMENTAL PROCEDURES

Protein Preparation. The full-length P450cam containing the C334A mutation was purified as described previously (18).

¹Abbreviations: rmsd, root-mean-square deviation; PCA, principal component analysis; P450cam-C, P450cam in the closed conformation; P450cam-I, P450cam in the intermediate open conformation; P450cam-O, P450cam in the open conformation; Pdx, putidaredoxin.

C334A has been shown to prevent intermolecular dimerization and increase protein stability but does not affect protein activity (30). Purified protein ($A_{417}/A_{280} > 1.45$) was exchanged into 50 mM KP_i (pH 6.0), 1 mM camphor, and 30 mM β -mercaptoethanol and frozen at -80 °C for further experiments.

Synthesis of Substrate Analogues. Reagents and solvents were purchased from commercial sources and used without further purification. Anhydrous *N,N*-diisopropylethylamine and DMF were purchased from Acros Organics. NMR spectra were recorded on a Varian Mercury 400 MHz spectrometer. The ¹H chemical shifts are expressed relative to the residual solvent signal. Mass spectra were recorded at the Scripps Research Institute Mass Spectrometry Facility. *tert*-Butyl 6-aminohexylcarbamate, *tert*-butyl 8-aminooctylcarbamate, and *tert*-butyl *N*-(2-[2-(2-aminoethoxy)ethoxy]ethyl)-carbamate were synthesized according to the procedure of Jaramillo et al. (31). The synthesis of AdaCl-C8-Dans was reported previously (32).

All Boc-protected adamantane-tethered substrate analogues were synthesized by the following general procedure (*tert*-butyl 8-aminooctylcarbamate and adamantyl carbonyl chloride are used as an illustrative example). *tert*-Butyl 8-aminooctylcarbamate (0.200 g, 0.822 mmol), adamantane 1-carbonyl chloride (0.196 g, 0.989 mmol), and 1 mL of *N,N*-diisopropylethylamine were dissolved in dry DMF (10 mL) under argon and stirred at room temperature overnight. The solvent was removed under reduced pressure, and the crude product was purified via flash chromatography (SiO₂) using a solvent gradient from 100% CH₂Cl₂ to a 9:1 CH₂Cl₂/MeOH mixture to give the product as a white solid. For the other adamantyl derivatives, the procedure was modified as follows: HOBt (hydroxybenzotriazole) (1.1 equiv) and EDC [1-ethyl-3-(3'-dimethylaminopropyl)carbodiimide] (1.1 equiv) were added to the reaction mixture.

The dansyl group was added to the adamantyl-tethered substrate analogues following deprotection of the Boc group using the following general procedure [1-(*tert*-butyl-8-aminooctylcarbamate) amidoadamantane is used as an illustrative example]. 1-(*tert*-Butyl-8-aminooctylcarbamate) amidoadamantane (0.100 g, 0.247 mmol) was dissolved in a 9:1 CH₂Cl₂/TFA mixture and stirred for 1 h at room temperature. The solvents were removed under reduced pressure, and the crude product was then dissolved in dry DMF (5 mL). *N,N*-Diisopropylethylamine (0.5 mL) was added, followed by dansyl chloride (0.100 g, 0.371 mmol). The reaction mixture was stirred under argon at room temperature overnight. The solvent was removed under reduced pressure, and the crude product was purified via flash chromatography (SiO₂) using gradient elution from CH₂Cl₂ (100%) to an 8:1:1 CH₂Cl₂/MeOH/Et₃N mixture as the eluent to give the product as a pale yellow solid.

Crystallization, Data Collection, and Crystal Structure Determination. Camphor was removed from protein stock solutions by buffer exchange into 20 mM Hepes (pH 6.5) by gel filtration through two sequential PD-10 columns (GE healthcare). P450cam (1 mM) was mixed with tethered substrate analogues (Table 1) in a 1:1 ratio. Crystals of P450cam bound to tethered substrates were grown by sitting-drop vapor diffusion at 6 °C from 100 mM cacodylic acid (pH 6.5), 12–22% polyethylene glycol 8000, and 200 mM K⁺. The crystals were transferred to cryoprotectant buffer consisting of 100 mM cacodylic acid (pH 6.5), 16–18% polyethylene glycol 8000, 25% polyethylene glycol 600, and 200 mM K⁺, mounted on nylon loops, and flash-frozen at 77 K.

X-ray diffraction data were collected at 100 K using beamline 7-1, 9-1, or 11-1 at the Stanford Synchrotron Radiation Laboratory.

Table 1: Structural Analysis of P450cam Conformers

Substrate ^a	PDB	PC1 ^b	PC2 ^b	F helix shift ^c (Å, deg)	G helix shift ^c (Å, deg)	FG helix angle (deg)	Axial Water	Missing B' helix	Ref
P450cam-C									
Camphor	2CPP	25.7	2.9	—	—	-148.9	No	—	(4)
	1YRC	29.4	4.9	0.28, 2.7	0.25, 2.8	-149.4			(42)
	5CP4	24.8	3.7	0.22, 2.7	0.40, 1.8	-150.1			(43)
	2ZAX	28.7	5.7	0.23, 3.1	0.28, 2.5	-148.7			(44)
	1DZ4	26.7	6.5	0.11, 1.2	0.55, 0.9	-150.1			(45)
1S-camphor	1AKD	23.9	6.1	0.41, 2.7	0.48, 1.4	-149.0	No	—	(46)
Imidazole	2H7Q	24.1	4.9	0.26, 2.2	0.54, 1.5	-151.4	No	—	(47)
Nicotine	1P2Y	25.9	5.6	0.08, 5.2	0.36, 0.5	-148.2	No	—	(48)
Metyrapone	1PHG	25.6	3.2	0.07, 1.4	0.12, 0.5	-148.6	No	—	(49)
P450cam-I									
AdaC1-C8-Dans	1RE9	6.4	-9.9	3.30, 17.8	1.00, 5.9	-156.6	No	—	(66)
	1LWL	4.4	-11.5	3.59, 17.4	1.33, 5.4	-156.5			(32)
	3P6M	2.7	-11.2	3.77, 15.5	1.52, 5.4	-156.7			This study
	3P6N	2.2	-11.1	3.75, 16.0	1.50, 6.2	-157.2			This study
AdaC1-C8EtgGlu-Bio	3OIA	3.0	-11.6	3.71, 15.8	1.27, 7.3	-153.2	No	—	Unpublished
AdaC1-Etg-Dans	3P6O	3.7	-10.6	3.73, 16.7	1.42, 6.0	-153.5	No	—	This study
AdaC1-C6-Bio	3P6P	2.5	-10.3	3.91, 15.2	1.37, 6.6	-157.8	No	—	This study
3OH-AdaC1-C8-Dans	3OL5	1.1	-10.5	3.88, 14.9	1.96, 5.1	-155.8	Yes	—	Unpublished
P450cam-O									
AdaC1-C4-Dans	1RF9	-9.9	0.7	3.94, 15.9	3.68, 10.8	-149.7	Yes	—	(66)
AdaC2-Etg-Boc	3P6Q	-15.6	3.2	4.51, 17.2	3.95, 15.2	—	Yes	92-95	This study
3OH-AdaC1-Etg-Boc	3P6R	-16.3	4.1	4.84, 16.6	4.57, 15.2	-151.1	No	90-96	This study
AdaC2-C8-Dans ^d	3P6S	-17.3	2.3	4.59, 17.1	4.46, 14.9	-150.2	No	—	This study
	3P6T	-15.5	0.7	4.24, 16.8	4.28, 15.7	-150.6			This study
AdaC3-C6-Dans	3P6U	-21.0	3.8	4.95, 17.8	4.83, 17.4	-150.6	Yes	93-94	This study
3Et-AdaC1-Etg-Boc	3P6V	-20.4	4.6	5.06, 17.4	5.02, 16.0	-150.7	No	90-96	This study
AdaC3-Etg-Boc	3P6W	-20.5	3.8	5.04, 17.1	4.85, 17.4	-151.0	No	91-95	This study
AdaC3-C8-Dans	3P6X	-22.2	3.9	5.07, 18.7	4.86, 18.1	-150.4	Yes	90-94	This study
AdaC1-perfluorobiphenyl-Ru(bipy) ₃	1K2O	-22.7	3.8	5.54, 21.0	5.14, 18.8	-151.6	Yes	—	(65)
AdaC1-C8-Ru(bipy) ₃	1QM0	-16.0	3.3	4.43, 16.0	4.28, 14.7	-149.0	Yes	—	(64)
Substrate-free	3L61	-24.9	4.3	5.27, 19.3	5.09, 17.9	-150.2	Yes	90-97	(18)
	3L62	-21.5	3.6	4.93, 18.2	4.73, 16.9	-150.2		91-94	(18)

^aWell-ordered electron density included for portions of the models colored red. ^bPC1 and PC2 are first two principal components in the PCA of crystal structures described in this table. ^cHelix shift is calculated relative to the camphor-bound closed conformation [Protein Data Bank (PDB) entry 2CPP] at the center of helix F (Lys178) and helix G (Lys197). ^dThe entire substrate was resolved only in the structure of PDB entry 3P6T.

Data were processed using Scala (33). Molecular replacement was conducted using Molrep (34) using the previously determined tethered substrate-bound P450cam structures (PDB entries 1RE9 and 1RF9). Model fitting and refinement were conducted with Coot (35) and Refmac5 (36), respectively. The final models were validated using Procheck (37), Sfcheck (38), Molprobity (39), and the PDB validation server. Statistics for data collection and refinement are listed in Table S1 of the Supporting Information. All structural graphics were generated using the Pymol Molecular Graphics System (40).

Structure Analysis. Structural superposition and principal component analysis were conducted with bio3d (41). A total of 30 crystal structures of P450cam bound to small substrates or tethered substrate analogues were aligned, and the coordinates of the C_{α} atoms were used as input for principal component analysis. Bound small substrates include camphor [PDB entries 2CPP (4), 1YRC (42), 5CP4 (43), 2ZAX (44), and 1DZ4 (45)], 1S-camphor [PDB entry 1AKD (46)], imidazole [PDB entry 2H7Q (47)], (S)-(-)-nicotine [PDB entry 1P2Y (48)], and metyrapone [PDB entry 1PHG (49)]. Chemical structures of all tethered substrate analogues used in this study and previously reported are summarized in Table 1. Helical displacement relative to the closed conformation (PDB entry 2CPP) was calculated on the basis of the coordinate difference in the C_{α} atoms at the helix center: Lys178 (helix F) and Lys197 (helix G). The rotation of the helix axes relative to the closed conformation (PDB entry 2CPP) was determined by calculation of the angle between the helix axes in the superimposed structures either at Lys178 or at Lys197. Helix axis parameters were determined using the algorithm implemented in HELO (50). The helix packing angle and the distance between helices F and G were determined using C-HELIX (51).

RESULTS

Structures of P450cam Bound to Tethered Substrates. The use of tethered substrate analogues allowed the trapping of a range of conformational states of the P450cam substrate access channel. X-ray crystal structures were determined for P450cam crystallized in the presence of each member of the library of tethered substrates listed in Table 1. These molecules contain adamantane substrate analogues tethered to surface-exposed groups by linkers of variable length and composition. In each case, the substrate binding channel was observed in an open conformation, in contrast to the closed camphor-bound state. For six of the new structures, the electron density was very well-defined for the complete length of the tethered substrate, and the well-ordered portions are colored red in Table 1. In other cases, additional electron density was apparent within the substrate channel compared with the solvent-filled open state of the substrate-free enzyme (18), and in addition, the axial water was absent from the distal heme face (Table 1). This suggests partial occupancy of the channel by these tethered substrates. In only two cases, AdaC2-Etg-Boc and AdaC3-C6-Dans, in which the axial water was present and the electron density was not well-resolved, was it not possible to verify occupation of the channel by the ligand. The most significant specific interaction observed between the tethered substrates and the protein is a hydrogen bond between Tyr96 and the carbonyl oxygen for those analogues containing the AdaC1 and AdaC2 linkage. The loss of this hydrogen bond appears to be related to the disorder of helix B', as residues in helix B' were not found in the electron density map of the most fully open structures (Table 1). Further analysis of the tethered substrate conformation

for these structures and its effects on the enzyme active site are described in a separate work.

The axial heme-bound water is absent in some tethered substrate-bound structures but is present in others (Table 1), and this variation is attributed to differences in protein conformation and the location and occupancy of substrates in the active site. For example, electron density for the water was not evident in the structures of P450cam-I with the exception of 3OH-AdaC1-C8-Dans, in which the hydroxyl of the tethered substrate forms a hydrogen bond with the axial water. On the other hand, the distal water was observed for most of the P450cam-O structures where the electron density for the substrates is less well-defined. This is consistent with previous observations that the axial water is displaced by tight-binding substrates (52). However, we cannot exclude the possibility that variation of distal heme water occupation results from partial X-ray-induced heme reduction for some structures. Such effects are unlikely the source of changes in the conformational state for the following reasons. While redox-dependent changes in backbone dynamics (53) and hydrogen–deuterium exchange rates (54) have been observed, these changes are most prevalent in helices B' and C rather than helices F and G. In addition, the camphor-bound ferrous P450cam structure has been shown to be very similar to the ferric form (45), and our structures of substrate-bound ferric enzyme are in good agreement with these closed conformations (18). Finally, the structure at 2.0 Å resolution for the dithionite-reduced P450cam in a complex with AdaC1-C8-Dans is identical to that of the ferric enzyme within an rmsd of 0.2 Å (unpublished data).

To determine whether crystal packing influences the resultant structures, protein–protein interfaces in the crystal were analyzed for all structures reported in this study. PISA analysis (55) verifies that the protein exists as a monomer in solution and that the largest packing interface in each conformational state varies between 500 and 700 Å², suggesting no extensive interface is present. The residues around the substrate channel involved in packing interactions with the neighboring molecules do not differ significantly (Figure S1 of the Supporting Information). In addition, the same unit cell (P212121) accommodates both P450cam-I and P450cam-O structures (Table S2 of the Supporting Information), and the exception to this unit cell (P21, PDB entry 1K2O) indicates that the P450cam-O conformation is not determined by the P212121 crystal form. Finally, the P450cam-C form exists in a variety of crystal forms (Table S2 of the Supporting Information), but the alternative lattices do not affect the protein conformation. All of these observations suggest the different structures in P450cam-O, -I, and -C do not result from differences in packing interactions.

Clusters of Protein Conformational States. The family of protein structures described above and determined previously displayed a distribution of conformations that range between the completely closed camphor-bound state (3) and the fully open form recently reported for P450cam crystallized in the absence of camphor (18). Overlaid in Figure 1A are 30 structures, including the 12 structures reported here (Table S1 of the Supporting Information) and 18 previously reported complexes. A range of protein conformational states are evident, with the most prominent rms fluctuations from the average structure occurring in helices B', F, and G and the F–G loop and to a lesser degree in helices C, H, and I (Figure 1B). It is also apparent that the variations in the substrate access channel appear to cluster into distinct families of conformations as indicated by the color scheme of Figure 1. As also indicated in Figure 1B, a number of regions adjacent to or in contact with helices F and G appear to undergo

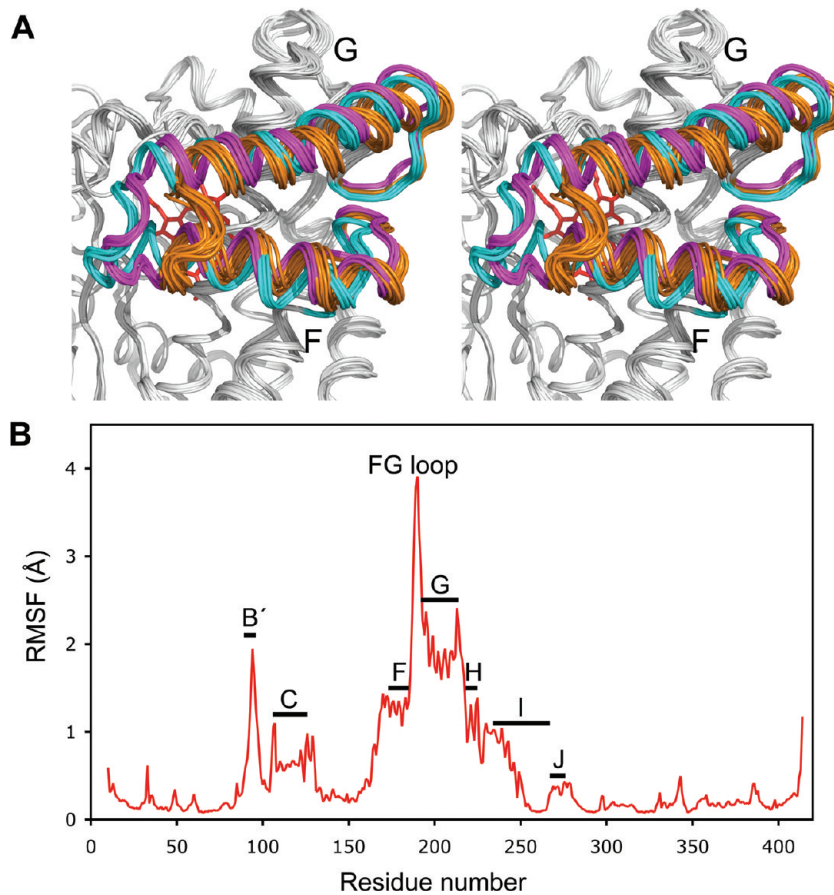


FIGURE 1: Crystal structures of P450cam bound to substrates listed in Table 1. (A) Stereoview of superimposed structures of the C_{α} backbone. (B) Average pairwise rmsd per residue (rmsf) along the sequence for these structures.

minimal fluctuations within this family of structures, suggesting that the conformational variations are highly localized to the elements defining the substrate binding channel. One exception is helix C, which is a part of the proposed putidaredoxin (Pdx) binding site (56).

Principal component analysis (PCA) of the combined set of structures shown in Figure 1 was used to characterize the range of observed conformational substates. PCA has been used to characterize differences within sets of both experimentally derived structures (57, 58) and those traversed in simulated molecular dynamics trajectories (59, 60). By reducing the number of correlated variables in multiple sets of structural coordinates to those that contribute most to the covariance, PCA has been useful in identifying the number and nature of the primary modes of protein dynamics. PCA of the combined set of P450cam structures described above shows that the first two principal components account for 93% of the covariance (Figure S2 of the Supporting Information) and thus provide a useful description of the conformational space sampled by the structural data. Figure 2A shows a plot of each of these structures projected onto the plane of the first two principal components (PC1 and PC2). The data are clearly clustered into three distinct groups, which we hereafter term P450cam-C (closed), P450cam-I (intermediate), and P450cam-O (open). The lack of additional clustering along the third principal component axis (Figure S2 of the Supporting Information) also indicates that the range of structural differences is described well by only the first two principal components. The P450cam-C cluster includes the previously well characterized closed conformation of the enzyme as typified by complexes with small molecule

inhibitors and substrates such as camphor (3, 46–49). At the other end of the range, at the left end of the P450cam-O cluster of Figure 2A, is the recently described open conformation seen in the absence of any substrate (18). It is particularly striking that the conformations for the library of tethered substrates are not evenly distributed across these extremes but instead fall into three distinct clusters of states.

PCA also provides insight into the nature of the structural differences among these three conformational substates. Shown in Figure 2B are the per-residue contributions to the structural changes for the first two principal components. Principal component 1 (PC1) and principal component 2 (PC2) involve similar contributions across several regions of the protein. The F–G loop and helix F make the largest contribution to both PC1 and PC2, indicating a highly covariational movement of these structural elements for either of these components. However, Figure 2B also shows distinct differences between PC1 and PC2, in which helix G makes a larger contribution to PC1 than it does to PC2. In addition, PC2 contains a larger contribution than PC1 for the H–I surface loop centered near Gly230 and a narrow region near Asp251 at the position of the bulge in the center of helix I. As seen in Figure 2A, the differences between the P450cam-C and P450cam-O conformational groups occur almost entirely with a change in PC1, while the P450cam-I states involve contributions from both PC1 and PC2. Thus, the difference between the fully closed P450cam-C and partially open P450cam-I conformations can be seen as arising from a complex coordinated movement involving helix F, the F–G and H–I surface loops, and helix I bulge, while helix G remains relatively unchanged. In contrast, the largest

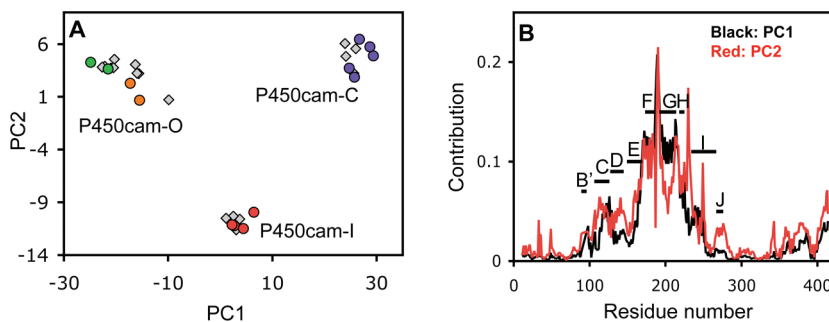


FIGURE 2: Principal component analysis of P450cam crystal structures. (A) Two-dimensional plot of the first two principal components for each structure. Data points representing repeat structures are colored differently: camphor (purple), AdaC1-C8-Dans (red), AdaC2-C8-Dans (orange), and substrate-free open (green) conformations. (B) Contribution of each residue in the sequence to the first (black) and second (red) principal components.

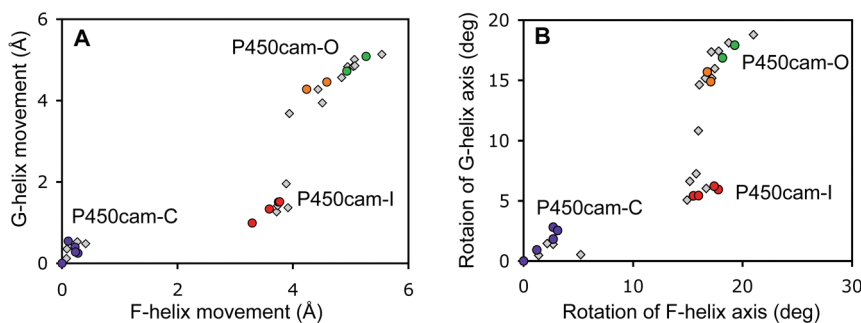


FIGURE 3: Geometric analysis of the movements of helices F and G of P450cam structures relative to that of the camphor-bound state (PDB entry 2CPP). Data points from repeat structures are colored as described in the legend of Figure 2. (A) Translational movement of helices F and G. (B) Rotation of the axis of helices F and G.

differences between P450cam-C and the fully open P450cam-O conformations involve a change in both helices F and G and the intervening F–G loop.

Specific displacements and relative orientations for helices F and G were examined for these structures to obtain a physical picture of the changes associated with the interconversion of the P450cam-C, P450cam-I, and P450cam-O states (graphical descriptions of these parameters are shown in Figure S3 of the Supporting Information). The mean helix displacement and orientation, measured at the helix midpoint, were calculated relative to the closed camphor-bound state (PDB entry 2CPP) and are plotted in Figure 3. As with PCA, the structures appear to be distributed into three clusters of conformations. Relative to the P450cam-C conformation, the P450cam-I intermediate results from an average retraction of helix F by 3.7 Å, while helix G moves in the same direction by only 1.5 Å. However, the difference between P450cam-C and P450cam-O results from larger and almost equal displacements of helices F and G of 4.8 and 4.9 Å, respectively. As shown in Figure 3B, a similar pattern is observed for the relative helix orientations. Because of distinct movements of helices F and G in the transition from the P450cam-C state to the P450cam-I and P450cam-O states, the F–G loop arrangement is different in the two open conformations. In P450cam-C, the F–G loop is bent toward the solvent accessible surface of helices F and G and hydrophilic interactions between residues in helix F and the F–G loop appear to stabilize this conformation (Figure S4 of the Supporting Information). However, in the P450cam-I state, movement of helix F leaves the F–G loop behind (Figure 1), and hydrophilic contacts are lost (Figure S4 of the Supporting Information). Despite significant changes in local contacts, backbone ϕ and ψ angles around the F–G loop are very similar in the three conformational states (Figure S5 of the Supporting Information).

Additional movement of helix G in the P450cam-O state eventually accompanies movement of the F–G loop with recovery of contacts between helix F and the F–G loop (Figure S4 of the Supporting Information). These observations indicate that the F–G loop moves as a unit and as part of helix G.

The scatter of structural coordinates for each cluster suggests that both P450cam-C and P450cam-I are well-defined states with a small distribution from the average, while P450cam-O represents a more widely distributed set of open conformations. In several cases, redundant structures were determined from separate crystals of the same protein–ligand combination, and these redundant structures are shown in the same color in Figures 2 and 3. The observed average standard deviations for displacement of helices F and G within the P450cam-C, P450cam-I, and P450cam-O clusters were 0.16, 0.24, and 0.46 Å, respectively, while that for the redundant structures was 0.18 Å. This suggests that P450cam-C and P450cam-I represent well-defined conformations in which individual structures do not vary by more than that seen for crystal-to-crystal variation, while the P450cam-O cluster is more broadly distributed over a range of open conformations. One previously reported ligand, AdaC1-C4-Dans, appeared at the boundary between P450cam-I and P450cam-O in the plot of rotations of helices F and G (Figure 3B).

Changes in Intraprotein Interactions. The distinct conformational states seen for P450cam result in a range of altered interactions between protein secondary structural elements. As the structure moves from the closed conformation to either of the open forms, a critical interaction between helix F and the bulge of helix I is disrupted. As shown in Figure 4, P450cam-C contains a bifurcated salt bridge between Lys178 and Arg186 in helix F and Asp251 in helix I. This salt bridge is lost in both the P450cam-I and P450cam-O conformations, resulting in the retraction of

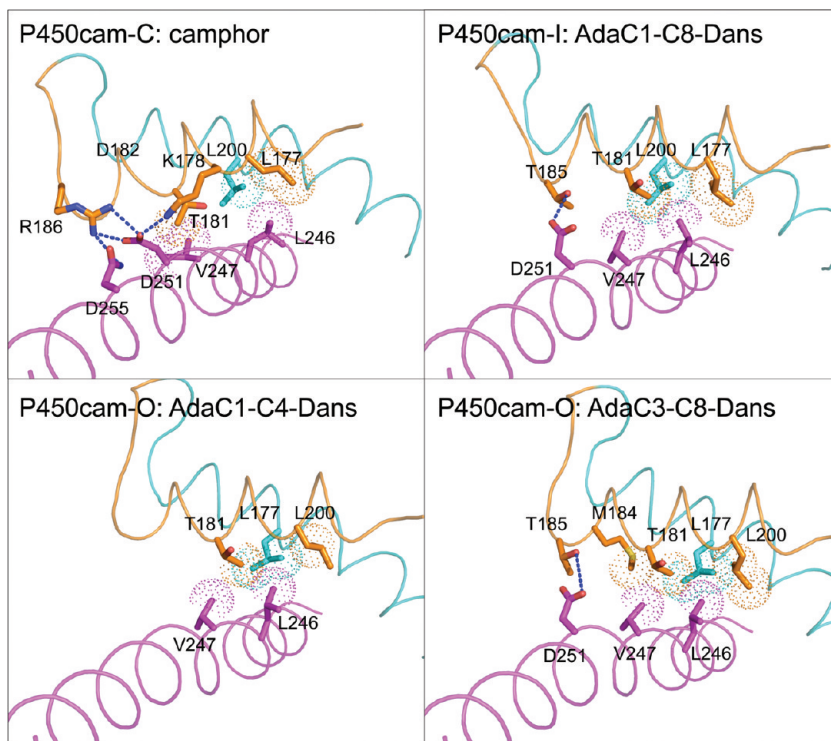


FIGURE 4: Interhelical contacts among helices F (orange), G (cyan), and I (magenta) shown for P450cam bound to camphor (P450cam-C), AdaC1-C8-Dans (P450cam-I), AdaC1-C4-Dans (P450cam-O), and AdaC3-C8-Dans (P450cam-O). Salt bridge and hydrogen bonding interactions are shown as blue dashes, while hydrophobic contacts are shown as dotted spheres.

helix F for both of these open conformations. Additional hydrophobic interactions among Leu177, Leu200, and Leu246 of helices F, G, and I are maintained in all three conformations, as they are near the point at which helix F pivots over helix I.

The loss of the salt bridge between helices F and I also accompanies changes in the bulge of helix I, which provides a pocket for O₂ and allows its hydrogen bonding to the catalytically important side chain of Thr252 (Figure 5) (61). In the P450cam-C state, the bulge of helix I results from the loss of the normal hydrogen bond acceptor (residues 249–251) and donor (residues 253–255) interactions (Figure 5). Because the bulge is shorter than one turn of the α -helix, helix I appears to be kinked in the middle (Figure S6 of the Supporting Information). When helix F retracts in the open conformations, the α -helical bulge is shifted toward the N-terminus of helix I and becomes distributed over almost two helical turns, and the distance between α -helical hydrogen donors and acceptors becomes shorter, but not enough to form hydrogen bonds. This shift results in a straightening of helix I (Figure S6 of the Supporting Information). Interestingly, because of this bulge shift, the distance between the normal Gly248 hydrogen bond acceptor and Thr252 donor increases from 3.7 Å (PDB entry 2CPP; P450cam-C) to 4.9 Å (PDB entry 3L62; P450cam-O). This, in turn, widens the α -helical groove near the active site and makes room for a “catalytic water” that is seen in the ferrous dioxygen-bound P450cam structure (45) (Figure S6 of the Supporting Information). Irrespective of the wider α -helical groove around Gly248 and Thr252, the unusual hydrogen bond between the Gly248 backbone carboxyl and the Thr252 side chain hydroxyl, which has been thought to be responsible for the bulge of helix I, was still preserved in each of the P450cam-I and P450cam-O conformations.

Helix G is seen to make a distinct switch in its interactions with other secondary structural elements in the protein as the channel

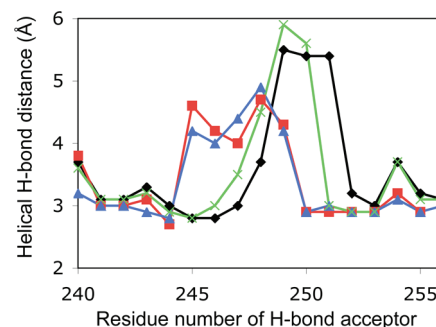


FIGURE 5: Geometrical analysis of the bulge of helix I. Distance between the hydrogen bond acceptor (residue *i*) and donor (residue *i* + 4) in helix I plotted for P450cam-C (black, PDB entry 2CPP), P450cam-I (red, PDB entry IRE9), P450cam-O (blue, PDB entry 3L62), and oxy-ferrous P450cam (green, PDB entry 1DZ8).

is converted from the closed P450cam-C state through the P450cam-I intermediate to the fully open P450cam-O state. As helix F initially retracts from P450cam-C to P450cam-I, helix G remains anchored by contacts with helix B' as shown in Figure 6. These contacts include a bifurcated hydrogen bond between Asp97 and two residues of helix G, Tyr201 and Lys197, and also hydrophobic interactions between Ala95 and Phe193 (Figure 6). These interactions appear to prevent helix G from following helix F as it retracts during the P450cam-C to P450cam-I transition. As the channel opens further during the P450cam-I to P450cam-O conversion, helix G finally retracts. However, as shown in Figure 6, for the interactions between helices G and B' to be maintained, helix B' itself unwinds, loses its K⁺ binding site, and becomes disordered, as recently described for the substrate-free open conformation (18). One structure, the complex with AdaC1-C4-Dans, which appears at the boundary between the P450cam-I

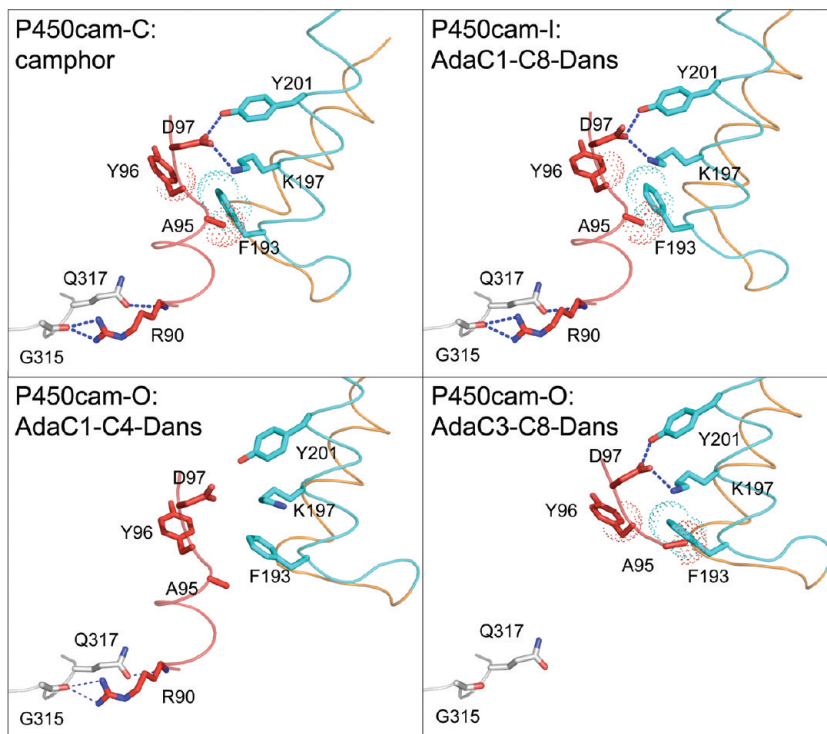


FIGURE 6: Interactions between helices B' and G shown for P450cam bound to camphor (P450cam-C), AdaC1-C8-Dans (P450cam-I), AdaC1-C4-Dans (P450cam-O), and AdaC3-C8-Dans (P450cam-O). Helices B', F, and G are colored red, orange, and cyan, respectively. Residues from strand β 3 are colored white. Electrostatic interactions are shown as blue dashes, while hydrophobic contacts are shown as dotted spheres.

and P450cam-O conformations, retains an ordered B' helix as helix G retracts, but it does this at the expense of breaking its interactions with helix G. As a result of the separate movements of helices F and G, the interhelical angle undergoes a small shift as one proceeds from P450cam-C to P450cam-I, but this angle is restored for the P450cam-O cluster (Figure S7 of the Supporting Information). Figure S7 also shows that helices F and G for P450cam-C and P450cam-O pack against each other in a classic antiparallel ridge-into-groove interaction with an interhelical angle of -150° (51). However, for the group of P450cam-I structures, the interhelical angle is reduced slightly to approximately -158° . As this interhelical angle changes during the P450cam-C to P450cam-I transition, several hydrophobic interactions between helices F and G are initially disrupted but are restored in P450cam-O (Figure S8 of the Supporting Information).

DISCUSSION

Conformational Clusters in P450cam. The process by which diverse P450s bind substrates and control the specificity and functional coupling of catalysis has been extensively studied (11, 62, 63). While some forms such as EryK (15) and PiKc (16) have been shown to exist in both closed and open states in the absence of substrates, the extent of structural changes traversed by a given enzyme during substrate binding is not well understood for any P450. Such changes are clearly necessary for some forms, most notably P450cam, which binds substrate in a completely closed solvent inaccessible conformation (3, 4). The open conformation observed for P450cam in the presence of large tethered substrates has demonstrated its ability to exist in open states (64–66), but only recently has this open conformation been observed in the absence of substrate (18). The open conformations of the substrate-free and the most open of the tethered substrate-bound forms are very similar (rmsd of 0.5 Å),

suggesting the open conformations observed for the tethered substrate-bound forms are not induced by the tethered substrates but are already preexisting in the conformational space of P450cam. Thus, examination of the range of structures exhibited while bound to a library of tethered substrate analogues may be very useful in revealing the distribution of conformational states sampled by the protein during substrate recognition and catalysis.

The 12 crystal structures presented here combined with analysis of 18 previously determined structures show how a wide variety of compounds are accommodated at the active site of P450cam. In response to the variation in the composition over the length of the tethered substrate, the protein displays a significant variation in the structure of the substrate access channel. However, the structures are not evenly distributed within this conformational space, as might be expected for a highly plastic substrate binding site, but are instead highly clustered into three families of states, P450cam-C, P450cam-I, and P450cam-O, indicating closed, intermediate, and fully open conformations, respectively. Both P450cam-C and P450cam-I appear to be well-defined states that show a narrow structural distribution that is not larger than that seen in repeat determinations of the same structure, while P450cam-O states are spread over a broader distribution, suggesting an ensemble of open conformations. The three conformations differ largely by movements of secondary structural elements that surround the substrate access channel, including helices B', F, G, and I. One exception to this is the small movement of helix C that forms part of the proposed Pdx binding site, suggesting that the enigmatic role of Pdx as a functional effector may be related to the conformational shifts involving the open to closed transition. Recent studies have suggested that Pdx binding forces selection of a closed conformational transition that prevents escape of substrate (67).

Each of the P450cam-O, P450cam-I, and P450cam-C conformational states is observed in the presence of multiple ligands

(Table 1). For example, the P450cam-O conformation, which is observed for substrate-free P450cam, lies within a 0.4 Å rmsd of that bound to the Ada-C2-Etg-Dans probe. In another example, the well-defined P450cam-I state is observed with a variety of ligands that vary over the substrate, linker, and surface resident positions (Table 1). Finally, a very narrow distribution is observed for all of the reported P450cam-C conformations despite accommodating a range of small substrates and inhibitors. On the other hand, minor differences in the tethered substrate composition are observed to cause significant changes in protein conformation. For example, AdaC1-C8-Dans and AdaC2-C8-Dans differ by only a single bond shift in the position of the amide linkage, yet this results in a significant shift from the P450cam-I state to the P450cam-O state (Table 1). Finally, the axial water ligand, associated with the spin state shift upon conversion to the camphor-bound state, is absent from each of the P450cam-C forms but is sometimes present and sometimes missing in both P450cam-I and P450cam-O (Table 1). These results show that a particular protein–substrate interaction does not always lead to a unique conformational outcome, and that each of the conformational states is able to accommodate a variety of probe molecules. Our analysis suggests that the protein displays an innate preference for a small number of preexisting conformational substates, and each of these states can accommodate a range of ligands without undergoing a continuous plastic response of the active site structure. This suggests that substrate recognition by P450cam occurs largely by conformational selection and is consistent with the conclusions of a recent study of CYP119 (29) and EryK (15).

Multistep Pathway for Channel Closure. Analysis of the library of structures presented here provides the basis for a proposed multistep pathway for closure of the substrate access channel around substrate. When each of the structures is displayed in a molecular animation ordered by the principal component displacement, the resulting movie (Supporting Information) gives a clear impression of a coordinated two-step trajectory involving a distinct half-open intermediate. As shown in the cartoon model in Figure 7, the P450cam-I state represents a distinct sequential intermediate in the stepwise closure of the channel (P450cam-O → P450cam-I → P450cam-C). Conversion of P450cam-O to P450cam-I occurs by closure of helix G over the active site, allowing the ordering of helix B' and creation of the K⁺ binding site, which has been shown to enhance camphor binding 10-fold (68). Final conversion from P450cam-I to P450cam-C involves further closure of helix F and formation of the salt bridge between Arg186 and Asp251. This later interaction is crucial for the formation of the well-known bulge of helix I that alters the positioning of Thr252 and a catalytic water at the active site (61). The fact that the bulge of helix I is significantly localized around Asp251 upon final closure from P450cam-I to P450cam-C may have significant mechanistic implications that will be explored in a separate publication.

Recent results have shown that the full range of conformations observed in this study is also sampled by adaptive accelerated molecular dynamics (69). Notably, beginning with P450cam-C, the simulations visit both P450cam-I and P450cam-O as distinct states during the molecular dynamics trajectory. This provides strong support that the experimentally determined family of structures described here represents snapshots of the conformational dynamics seen in this enzyme.

In conclusion, the structures presented here show that P450cam samples at least three distinct conformational states and suggests that substrate recognition occurs by a process involving an

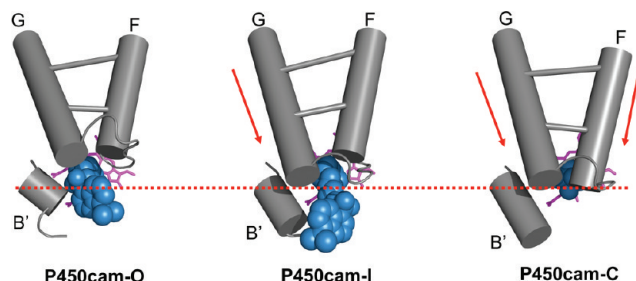


FIGURE 7: Model for the multistep closure of P450cam. Helices are represented as cylinders. Tethered substrates are shown as a CPK model colored blue: camphor (P450cam-C), AdaC1-C8-Dans (P450cam-I), and AdaC1-C4-Dans (P450cam-O). Heme is colored magenta. A red dashed line was drawn to help track changes between conformational states.

ordered multistep closure of the P450cam-O conformation around the substrate by way of a well-defined intermediate structure, P450cam-I. At present, it is not clear if the P450cam-I or P450cam-O conformations are catalytically competent. However, the discrete conformational states observed for the 30 P450cam structures analyzed in this study suggest that the initial interaction of camphor with P450cam-O results in a shift in equilibrium from P450cam-O to P450cam-I by conformational selection. Subsequent conversion to P450cam-C could also involve selection of substrate orientation within the channel, which may guide the protein over conformational barriers between preexisting conformations.

ACKNOWLEDGMENT

We thank Dr. A. Annalora for valuable discussions. We also thank the staff at the Stanford Synchrotron Radiation Light-source, a national user facility operated by Stanford University on behalf of the U.S. Department of Energy, Office of Basic Energy Sciences. The Stanford Synchrotron Radiation Light-source is supported by the Department of Energy, Office of Biological and Environmental Research, by the National Institutes of Health, National Center for Research Resources, Biomedical Technology Program, and by the National Institute of General Medical Sciences.

SUPPORTING INFORMATION AVAILABLE

X-ray crystallographic statistics for all structures reported in this study (Table S1), crystal packing interface around the substrate channel (Figure S1), two-dimensional plots of the first three principal components and the magnitude of covariance from each principal component (Figure S2), graphical description of geometrical parameters analyzed in this study (Figure S3), analysis of contacts around the F–G loop (Figure S4), backbone angles around the F–G loop (Figure S5), geometry of the bulge of helix I (Figure S6); analysis of packing angles and distances between helices F and G in P450cam structures (Figure S7), analysis of contacts between helices F and G for P450cam-C, P450cam-I, and P450cam-O (Figure S8), and an animated video showing a proposed model of the substrate channel opening. This material is available free of charge via the Internet at <http://pubs.acs.org>.

REFERENCES

- Nelson, D. R. (2009) The cytochrome p450 homepage. *Hum. Genomics* 4, 59–65.
- Guengerich, F. P. (2005) Human cytochrome P450 enzymes. In *Cytochrome P-450: Structure, Mechanism, and Biochemistry* (Ortiz de Montellano, P. R., Ed.) 3rd ed., pp 377–530, Kluwer Academic/Plenum, New York.

3. Poulos, T. L., Finzel, B. C., Gunsalus, I. C., Wagner, G. C., and Kraut, J. (1985) The 2.6-Å crystal structure of *Pseudomonas putida* cytochrome P-450. *J. Biol. Chem.* **260**, 16122–16130.
4. Poulos, T. L., Finzel, B. C., and Howard, A. J. (1987) High-resolution crystal structure of cytochrome P450cam. *J. Mol. Biol.* **195**, 687–700.
5. Johnson, E. F., and Stout, C. D. (2005) Structural diversity of human xenobiotic-metabolizing cytochrome P450 monooxygenases. *Biochem. Biophys. Res. Commun.* **338**, 331–336.
6. Poulos, T. L., and Johnson, E. F. (2005) Structures of cytochrome P450 enzymes. In Cytochrome P-450: Structure, Mechanism, and Biochemistry (Ortiz de Montellano, P. R., Ed.) 3rd ed., pp 87–114. Kluwer Academic/Plenum, New York.
7. Groves, J. T. (1985) Key elements of the chemistry of cytochrome P-450: The oxygen rebound mechanism. *J. Chem. Educ.* **62**, 928–931.
8. Gotoh, O. (1992) Substrate recognition sites in cytochrome P450 family 2 (CYP2) proteins inferred from comparative analyses of amino acid and coding nucleotide sequences. *J. Biol. Chem.* **267**, 83–90.
9. Pochapsky, T. C., Kazanis, S., and Dang, M. (2010) Conformational plasticity and structure/function relationships in cytochromes P450. *Antioxid. Redox Signaling* **13**, 1273–1296.
10. Meharennna, Y. T., Li, H., Hawkes, D. B., Pearson, A. G., De Voss, J., and Poulos, T. L. (2004) Crystal structure of P450cin in a complex with its substrate, 1,8-cineole, a close structural homologue to D-camphor, the substrate for P450cam. *Biochemistry* **43**, 9487–9494.
11. Pylypenko, O., and Schlichting, I. (2004) Structural aspects of ligand binding to and electron transfer in bacterial and fungal P450s. *Annu. Rev. Biochem.* **73**, 991–1018.
12. Poulos, T. L., Cupp-Vickery, J., and Li, H. (1995) Structural studies on prokaryotic cytochromes P450. In Cytochrome P-450: Structure, Mechanism, and Biochemistry (Ortiz de Montellano, P. R., Ed.) 2nd ed., pp 125–150. Plenum Press, New York.
13. Scott, E. E., He, Y. A., Wester, M. R., White, M. A., Chin, C. C., Halpert, J. R., Johnson, E. F., and Stout, C. D. (2003) An open conformation of mammalian cytochrome P450 2B4 at 1.6-Å resolution. *Proc. Natl. Acad. Sci. U.S.A.* **100**, 13196–13201.
14. Scott, E. E., White, M. A., He, Y. A., Johnson, E. F., Stout, C. D., and Halpert, J. R. (2004) Structure of mammalian cytochrome P450 2B4 complexed with 4-(4-chlorophenyl)imidazole at 1.9-Å resolution: Insight into the range of P450 conformations and the coordination of redox partner binding. *J. Biol. Chem.* **279**, 27294–27301.
15. Savino, C., Montemiglio, L. C., Sciarra, G., Miele, A. E., Kendrew, S. G., Jemth, P., Gianni, S., and Vallone, B. (2009) Investigating the structural plasticity of a cytochrome P450: Three dimensional structures of P450 EryK and binding to its physiological substrate. *J. Biol. Chem.* **284**, 29170–29179.
16. Sherman, D. H., Li, S., Yermalitskaya, L. V., Kim, Y., Smith, J. A., Waterman, M. R., and Podust, L. M. (2006) The structural basis for substrate anchoring, active site selectivity, and product formation by P450 PtkC from *Streptomyces venezuelae*. *J. Biol. Chem.* **281**, 26289–26297.
17. Zhao, Y. H., White, M. A., Muralidhara, B. K., Sun, L., Halpert, J. R., and Stout, C. D. (2006) Structure of microsomal cytochrome P450B4 complexed with the antifungal drug bifonazole: Insight into p450 conformational plasticity and membrane interaction. *J. Biol. Chem.* **281**, 5973–5981.
18. Lee, Y.-T., Wilson, R. F., Rupniewski, I., and Goodin, D. B. (2010) P450cam visits an open conformation in the absence of substrate. *Biochemistry* **49**, 3412–3419.
19. Li, H., and Poulos, T. L. (1997) The structure of the cytochrome p450BM-3 haem domain complexed with the fatty acid substrate, palmitoleic acid. *Nat. Struct. Biol.* **4**, 140–146.
20. Zhao, B., Guengerich, F. P., Bellamine, A., Lamb, D. C., Izumikawa, M., Lei, L., Podust, L. M., Sundaramoorthy, M., Kalaitzis, J. A., Reddy, L. M., Kelly, S. L., Moore, B. S., Stec, D., Voehler, M., Falck, J. R., Shimada, T., and Waterman, M. R. (2005) Binding of two flaviolin substrate molecules, oxidative coupling, and crystal structure of *Streptomyces coelicolor* A3₂ cytochrome P450 158A2. *J. Biol. Chem.* **280**, 11599–11607.
21. Park, S. Y., Yamane, K., Adachi, S., Shiro, Y., Weiss, K. E., Maves, S. A., and Sligar, S. G. (2002) Thermophilic cytochrome P450 (CYP119) from *Sulfolobus solfataricus*: High resolution structure and functional properties. *J. Inorg. Biochem.* **91**, 491–501.
22. Xu, L. H., Fushinobu, S., Ikeda, H., Wakagi, T., and Shoun, H. (2009) Crystal structures of cytochrome P450 105P1 from *Streptomyces avermitilis*: Conformational flexibility and histidine ligation state. *J. Bacteriol.* **191**, 1211–1219.
23. Ouellet, H., Podust, L. M., and de Montellano, P. R. O. (2008) *Mycobacterium tuberculosis* CYP130: Crystal structure, biophysical characterization, and interactions with antifungal azole drugs. *J. Biol. Chem.* **283**, 5069–5080.
24. Zerbe, K., Pylypenko, O., Vitali, F., Zhang, W., Rouset, S., Heck, M., Vrijbloed, J. W., Bischoff, D., Bister, B., Süßmuth, R. D., Pelzer, S., Wohlleben, W., Robinson, J. A., and Schlichting, I. (2002) Crystal structure of OxyB, a cytochrome P450 implicated in an oxidative phenol coupling reaction during vancomycin biosynthesis. *J. Biol. Chem.* **277**, 47476–47485.
25. Poulos, T. L., Finzel, B. C., and Howard, A. J. (1986) Crystal structure of substrate-free *Pseudomonas putida* cytochrome P-450. *Biochemistry* **25**, 5314–5322.
26. Williams, P. A., Cosme, J., Vinkovic, D. M., Ward, A., Angove, H. C., Day, P. J., Vonrhein, C., Tickle, I. J., and Jhoti, H. (2004) Crystal structures of human cytochrome P450 3A4 bound to metyrapone and progesterone. *Science* **305**, 683–686.
27. Annalora, A. J., Goodin, D. B., Hong, W., Zhang, Q., Johnson, E. F., and Stout, C. D. (2010) The crystal structure of CYP24A1, a mitochondrial cytochrome P450 involved in vitamin D metabolism. *J. Mol. Biol.* **396**, 441–451.
28. Boehr, D. D., Nussinov, R., and Wright, P. E. (2009) The role of dynamic conformational ensembles in biomolecular recognition. *Nat. Chem. Biol.* **5**, 789–796.
29. Lampe, J. N., Brandman, R., Sivaramakrishnan, S., and Ortiz de Montellano, P. R. (2010) 2D NMR and all-atom molecular dynamics of cytochrome P450 CYP119 reveal hidden conformational substates. *J. Biol. Chem.* **285**, 9594–9603.
30. Nickerson, D. P., and Wong, L. L. (1997) The dimerization of *Pseudomonas putida* cytochrome P450cam: Practical consequences and engineering of a monomeric enzyme. *Protein Eng.* **10**, 1357–1361.
31. Jaramillo, D., Wheate, N. J., Ralph, S. F., Howard, W. A., Tor, Y., and Aldrich-Wright, J. R. (2006) Polyamide platinum anticancer complexes designed to target specific DNA sequences. *Inorg. Chem.* **45**, 6004–6013.
32. Dunn, A. R., Hays, A. M., Goodin, D. B., Stout, C. D., Chiu, R., Winkler, J. R., and Gray, H. B. (2002) Fluorescent probes for cytochrome p450 structural characterization and inhibitor screening. *J. Am. Chem. Soc.* **124**, 10254–10255.
33. Evans, P. R. (1993) Data reduction. *CCP4 Study Weekend Proceedings DL/SCI/R34*, 114–122.
34. Vagin, A., and Teplyakov, A. (1997) MOLREP: An automated program for molecular replacement. *J. Appl. Crystallogr.* **30**, 1022–1025.
35. Emsley, P., and Cowtan, K. (2004) Coot: Model-building tools for molecular graphics. *Acta Crystallogr. D60*, 2126–2132.
36. Murshudov, G. N., Vagin, A. A., and Dodson, E. J. (1997) Refinement of macromolecular structures by the maximum-likelihood method. *Acta Crystallogr. D53*, 240–255.
37. Laskowski, R. A., MacArthur, M. W., Moss, D. S., and Thornton, J. M. (1993) Procheck: A Program to Check the Stereochemical Quality of Protein Structures. *J. Appl. Crystallogr.* **26**, 283–291.
38. Vaguine, A. A., Richelle, J., and Wodak, S. J. (1999) SFCHECK: A unified set of procedures for evaluating the quality of macromolecular structure-factor data and their agreement with the atomic model. *Acta Crystallogr. D55*, 191–205.
39. Lovell, S. C., Davis, I. W., Adrendall, W. B., de Bakker, P. I. W., Word, J. M., Prisant, M. G., Richardson, J. S., and Richardson, D. C. (2003) Structure validation by Cα geometry: ϕ , ψ and Cβ deviation. *Proteins* **50**, 437–450.
40. DeLano, W. L. (2002) The PyMOL Molecular Graphics System, DeLano Scientific, Palo Alto, CA.
41. Grant, B. J., Rodrigues, A. P. C., ElSawy, K. M., McCammon, J. A., and Caves, L. S. D. (2006) Bio3d: An R package for the comparative analysis of protein structures. *Bioinformatics* **22**, 2695–2696.
42. Meilleur, F., Dauvergne, M. T., Schlichting, I., and Myles, D. A. (2005) Production and X-ray crystallographic analysis of fully deuterated cytochrome P450cam. *Acta Crystallogr. D61*, 539–544.
43. Vidakovic, M., Sligar, S. G., Li, H., and Poulos, T. L. (1998) Understanding the role of the essential Asp251 in cytochrome p450cam using site-directed mutagenesis, crystallography, and kinetic solvent isotope effect. *Biochemistry* **37**, 9211–9219.
44. Harada, K., Sakurai, K., Ikemura, K., Ogura, T., Hirota, S., Shimada, H., and Hayashi, T. (2008) Evaluation of the functional role of the heme-6-propionate side chain in cytochrome P450cam. *J. Am. Chem. Soc.* **130**, 432–433.
45. Schlichting, I., Berendzen, J., Chu, K., Stock, A. M., Maves, S. A., Benson, D. E., Sweet, R. M., Ringe, D., Petsko, G. A., and Sligar, S. G. (2000) The catalytic pathway of cytochrome p450cam at atomic resolution. *Science* **287**, 1615–1622.

46. Schlichting, I., Jung, C., and Schulze, H. (1997) Crystal structure of cytochrome P-450cam complexed with the (1S)-camphor enantiomer. *FEBS Lett.* **415**, 253–257.
47. Verras, A., Alian, A., and de Montellano, P. R. (2006) Cytochrome P450 active site plasticity: Attenuation of imidazole binding in cytochrome P450(cam) by an L244A mutation. *Protein Eng., Des. Sel.* **19**, 491–496.
48. Strickler, M., Goldstein, B. M., Maxfield, K., Shireman, L., Kim, G., Matteson, D. S., and Jones, J. P. (2003) Crystallographic studies on the complex behavior of nicotine binding to P450cam (CYP101). *Biochemistry* **42**, 11943–11950.
49. Poulos, T. L., and Howard, A. J. (1987) Crystal structures of metyrapone- and phenylimidazole-inhibited complexes of cytochrome P-450cam. *Biochemistry* **26**, 8165–8174.
50. Tatulian, S. A. (2008) Determination of helix orientations in proteins. *Comput. Biol. Chem.* **32**, 370–374.
51. Dalton, J. A., Michalopoulos, I., and Westhead, D. R. (2003) Calculation of helix packing angles in protein structures. *Bioinformatics* **19**, 1298–1299.
52. Raag, R., and Poulos, T. L. (1991) Crystal structures of cytochrome P-450CAM complexed with camphane, thiocamphor, and adamantane: Factors controlling P-450 substrate hydroxylation. *Biochemistry* **30**, 2674–2684.
53. Pochapsky, S. S., Dang, M., Ouyang, B., Simorellis, A. K., and Pochapsky, T. C. (2009) Redox-Dependent Dynamics in Cytochrome P450(cam). *Biochemistry* **48**, 4254–4261.
54. Hamuro, Y., Molnar, K. S., Coales, S. J., OuYang, B., Simorellis, A. K., and Pochapsky, T. C. (2008) Hydrogen-deuterium exchange mass spectrometry for investigation of backbone dynamics of oxidized and reduced cytochrome P450cam. *J. Inorg. Biochem.* **102**, 364–370.
55. Krissinel, E., and Henrick, K. (2007) Inference of macromolecular assemblies from crystalline state. *J. Mol. Biol.* **372**, 774–797.
56. Pochapsky, T. C., Lyons, T. A., Kazanis, S., Arakaki, T., and Ratnawamy, G. (1996) A structure-based model for cytochrome P450cam-putidaredoxin interactions. *Biochimie* **78**, 723–733.
57. Grant, B. J., McCammon, J. A., Caves, L. S., and Cross, R. A. (2007) Multivariate analysis of conserved sequence-structure relationships in kinesins: Coupling of the active site and a tubulin-binding subdomain. *J. Mol. Biol.* **368**, 1231–1248.
58. Teodoro, M. L., Phillips, G. N., and Kavraki, L. E. (2003) Understanding protein flexibility through dimensionality reduction. *J. Comput. Biol.* **10**, 617–634.
59. Amadei, A., Linssen, A. B., and Berendsen, H. J. (1993) Essential dynamics of proteins. *Proteins* **17**, 412–425.
60. Amadei, A., Linssen, A. B., de Groot, B. L., van Aalten, D. M., and Berendsen, H. J. (1996) An efficient method for sampling the essential subspace of proteins. *J. Biomol. Struct. Dyn.* **13**, 615–625.
61. Nagano, S., and Poulos, T. L. (2005) Crystallographic study on the dioxygen complex of wild-type and mutant cytochrome P450cam. Implications for the dioxygen activation mechanism. *J. Biol. Chem.* **280**, 31659–31663.
62. Denisov, I. G., Makris, T. M., Sligar, S. G., and Schlichting, I. (2005) Structure and chemistry of cytochrome P450. *Chem. Rev.* **105**, 2253–2277.
63. Isin, E. M., and Guengerich, F. P. (2008) Substrate binding to cytochromes P450. *Anal. Bioanal. Chem.* **392**, 1019–1030.
64. Dmochowski, I. J., Crane, B. R., Wilker, J. J., Winkler, J. R., and Gray, H. B. (1999) Optical detection of cytochrome P450 by sensitizer-linked substrates. *Proc. Natl. Acad. Sci. U.S.A.* **96**, 12987–12990.
65. Dunn, A. R., Dmochowski, I. J., Bilwes, A. M., Gray, H. B., and Crane, B. R. (2001) Probing the open state of cytochrome P450cam with ruthenium-linker substrates. *Proc. Natl. Acad. Sci. U.S.A.* **98**, 12420–12425.
66. Hays, A. M. A., Dunn, A. R., Chiu, R., Gray, H. B., Stout, C. D., and Goodin, D. B. (2004) Conformational states of cytochrome P450cam revealed by trapping of synthetic molecular wires. *J. Mol. Biol.* **344**, 455–469.
67. Asciutto, E. K., Madura, J. D., Pochapsky, S. S., Ouyang, B., and Pochapsky, T. C. (2009) Structural and Dynamic Implications of an Effector-Induced Backbone Amide cis-trans Isomerization in Cytochrome P450(cam). *J. Mol. Biol.* **388**, 801–814.
68. Di Primo, C., Hui Bon Hoa, G., Douzou, P., and Sligar, S. (1990) Mutagenesis of a single hydrogen bond in cytochrome P-450 alters cation binding and heme solvation. *J. Biol. Chem.* **265**, 5361–5363.
69. Markwick, P. R., Pierce, L. C., Goodin, D. B., and McCammon, J. A. (2011) Adaptive accelerated molecular dynamics (Ad-AMD) reveals the molecular plasticity of P450cam (manuscript submitted for publication).